CHEMISTRY OF MATERIALS

ARTICLE

pubs.acs.org/cm

New Mixed Ligand Single-Source Precursors for PbS Nanoparticles and Their Solvothermal Decomposition to Anisotropic Nano- And Microstructures

Trinanjana Mandal,[†] Graham Piburn,[†] Vitalie Stavila,[†,‡] Irene Rusakova,[§] Teyeb Ould-Ely,[†,⊥] Adam C. Colson,[†] and Kenton H. Whitmire*[,†]

[†]Department of Chemistry, MS-60, Rice University, 6100 Main Street, Houston, Texas 77005, United States

[§]Texas Center for Superconductivity, University of Houston (TcSUH), HSC Building, University of Houston, Texas 77204-5002, United States

Supporting Information

ABSTRACT: Six new precursors for lead sulfide nanoparticles were synthesized by the reaction of lead acetate, with picolinic (Hpic), 2,6-dipicolinic (H_2dipic) or salicylic (H_2sal) acid followed by the addition of thiourea (tu) or thiosemicarbazide (ths). The compounds are "[Pb(Hsal)$_2$(tu)$_2$]" (**1a**), "Pb(Hsal)$_2$-(ths)$_3$·2H_2O" (**1b**), "Pb(pic)$_2$(tu)" (**2a**), [Pb(pic)$_2$(ths)$_2$]$_2$ (**2b**), [Pb(dipic)(tu)(H_2O)]$_2$·2H_2O (**3a**), and [Pb(dipic)(ths)$_2$]·2H_2O (**3b**). Compounds **2b**, **3a**, and **3b** formed well-defined crystals and were characterized by single-crystal X-ray diffraction, while the remaining compounds were characterized spectroscopically and by elemental analyses. The precursors were decomposed in both aqueous and nonaqueous media leading to pure crystalline galena in all cases. Depending upon conditions truncated octahedra, dendrites, nanocubes, interlinked nanocubes, nanohexapods and cubes were obtained. To elucidate the effect of single-source precursors on the mechanism of growth of nanoparticles, we compared the decomposition results with PbS nanostructures synthesized from multiple-source precursors using lead acetate with thiourea or thiosemicarbazide.

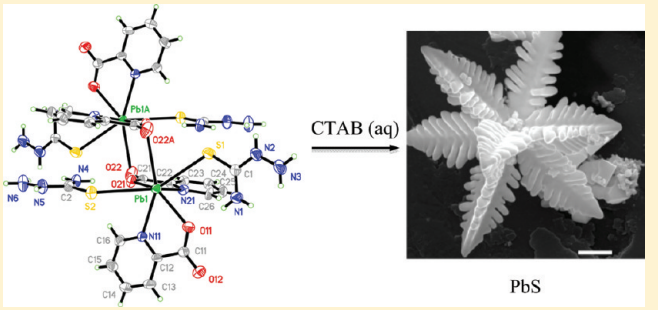

KEYWORDS: lead sulfide, nanoparticle, semiconductor, solvothermal, picolinate, dipicolinate, salicylate, thiourea, thiosemicarbazide

INTRODUCTION

In recent years the scientific community has discovered nature's ability to produce nano- and microstructures with extended length scale and displaying unique performance and architectures unmatched by today's engineering.[1] These nano- and microarchitectures can grow anisotropically in one, two, or three dimensions. To mimic nature's ability to construct architectures with extended length scale, one needs to consider two opposing factors; (1) crystal growth (or faceting) and (2) crystal dissolution such as Ostwald ripening or polymorph interconversion.[2] Dissolution in particular is a valuable mechanism for etching and exposing crystal planes and generating crystal shapes that are not easily obtained through growth alone.[3]

Polymorphs of the same substance usually have different physical and chemical properties, such as solubility, melting point, color, bioavailability, and compressibility.[4] Thus, the ability to integrate anisotropy in a single nanoarchitecture may yield new categories of smart nanomaterials. It is therefore of prime importance to combine and control these two aspects of crystal growth; the faceting (which is often determined at the nucleation stage), and the dissolution (which takes place during growth). To probe the importance of these two phenomena in crystal shape engineering and with the aim of producing nanostructures with extended length scale, we investigated a wide range of experimental conditions such as single-source precursors compared to multiple-source precursors and growth in aqueous as opposed to organic media.

PbS was selected because of its technological properties that range from solar light harvesting to near-IR communication, optical switches, thermal and biological imaging.[5] It is one of the most explored materials with several different morphologies of PbS nanocrystals having been synthesized by various methods. Nanometer- to micrometer-sized cubes, stars, rods, wires, and hexapods have been synthesized via thermal or solvothermal decomposition of single or multiple- source precursors in presence of different surfactants. Nanorods have been prepared in surfactant and polymer assisted template method.[6] Bierman et al. have reported a chemical vapor deposition technique using hydrogen gas as a vapor−liquid−solid (VLS) catalyst to generate hyperbranched PbS nanowires.[7] Aerosol -assisted chemical vapor deposition technique has been used by O'Brien and colleagues to

Received: April 13, 2011
Revised: August 21, 2011
Published: September 02, 2011

generate thin films of PbS nanocrystals from single-source precursors.[8] Solution-liquid−solid (SLS) growth starting from single-source precursors has been reported by two separate groups.[9] Alivisatos and co-workers have reported a synthetic strategy where a sequential cation exchange reaction has been utilized to generate anisotropic PbS nanorods.[10] There have been sonochemical and electrosonochemical approaches to synthesize PbS nanoparticles using capping agents like polyvinyl alcohol (PVA) or polyethylene glycol (PEG) either by direct high-intensity ultrasound irradiation or by carrying out the electrolysis under ultrasonic field.[11] Unconventional shapes like triangles and pyramids have been synthesized at the air−water interface via reaction between Pb^{2+} and H_2S gas in PVK (poly-9-vinylcarbazole) thin films.[12] PbS nanoparticle superlattices have been generated by direct templating in organic lyotropic liquid crystals and in ionic liquids.[13]

Among the methods mentioned above solvothermal synthesis of PbS nanoparticles has attracted much interest. The flexibility of incorporating different additives in the system such as surfactants, polymers, biomacromolecules, coordinating ligands or inorganic ions provide a simple way of generating variable nano- to submicrometer-sized particles. We have been exploring solvothermal decompositions of novel single-source precursors for synthesizing PbS nanoparticles.

Several advantages of using a single-source precursor have been demonstrated by our group as well as other researchers previously.[8,9,14] Intimate mixing in the molecular level ensures product homogeneity. Furthermore, the bridging or chelating organic ligands help preventing molecular segregation and the loss of the volatile organic moiety in the course of decomposition may impart unusual or desirable structural features in the end product such as high surface area, low density, connected channels or the formation of metastable phases.[14c,15] In addition, the strength of binding of the ligands on single-source metal precursor can be employed to tune the decomposition kinetics of the complex.

The use of different single-source precursors has been reported for the synthesis of PbS nanostructures. Dialkyldithiocarbamate compounds of Pb(II) are well-known in this regard. O'Brien and co-workers have reported the use of various different dialkyldithiocarbamates $[Pb(S_2CNRR')_2]$ (where R = Me, dioctyl, Et, ^{n}Pr) and R′ = benzyl, heptyl, octadecyl, dioctyl, Hex, Me, Et, and ^{n}Pr) to synthesize PbS thin films on glass substrates by chemical vapor deposition.[8] Buhro et al. have reported use of diethyldithiocarbamate compound of Pb(II) in a solution-liquid−solid (SLS) synthesis of PbS nanorods using Bi as catalyst.[9b] In a more recent approach, Jen-La Plante et al. have used another dialkyldithiocarbamate (R = R′= C_4H_{10}) compound of Pb(II) in a slightly modified solution−liquid−solid (SLS) synthesis of rectangular sheets and branched dendritic stars of PbS.[9a] O'Brien and co-workers have reported the use of $[Pb(S_2(P(C_6H_5)_2)_2N)]$ as a precursor for solvothermal decomposition under elevated pressure.[16] Boudjouk et al. have reported the pyrolysis of lead bis(benzylthiolates) to prepare PbS nanocrystals.[14a] Duan et al. have reported the use of lead dialkyldithiophosphates as single source precursors giving rise to PbS nanocubes under solvothermal decomposition.[14b] Two coordination polymers of Pb and nicotinic acid (Nic), $[Pb(2\text{-Nic})(NCS)]_n$ and $[Pb(3\text{-Nic})(NCS)]_n$, have been synthesized and utilized as precursors to synthesize nanorods and nanoplates via calcination.[17] Lead thiobenzoates used as single-source precursors gave rise to dendritic stars when decomposed with ethylenediamine, whereas use of bis(thiosemicarbazide) lead complexes generated dendritic stars on hydrothermal decomposition.[18]

Decomposing the same precursor (single or multiple sources) in both aqueous and organic media with the intent of combining faceted and dissolution growth to produce extended length scale has not been reported to our knowledge. Table 3 shows a comparison of the different single-source precursors previously reported in literature and herein. A further goal was to achieve decomposition to well-shaped nanoparticles without the need for addition of sulfur-containing ligands.

Precursor complexes based on salicylic (H_2sal), picolinic (Hpic), and 2,6-dipicolinic (H_2dipic) acids were natural choices as they can coordinate as multidentate ligands to form stable complexes that nevertheless decompose relatively readily. At the same time, the different binding strengths of the ligands can provide a means of controlling the kinetics of decomposition and hence the nanocrystal morphology. As a sulfur source, thiourea and thiosemicarbazide were chosen for study as these molecules form stable coordination bonds with the Pb through the S and sometimes also the N center. We have also investigated the mechanism of formation of PbS NPs of various shapes and sizes

Table 1. X-ray Crystallographic Structure Parameters for 2b, 3a and 3b

	2b	3a	3b
formula	$C_{28}H_{36}N_{16}O_8Pb_2S_4$	$C_{16}H_{22}N_6O_{12}Pb_2S_2$	$C_9H_{17}N_7O_6PbS_2$
fw	633.67	450.43	566.58
cryst syst	triclinic	monoclinic	monoclinic
space group	$P\bar{1}$	$P2_1/a$	$P2/c$
a (Å)	9.3237(19)	6.5197(4)	10.593(2)
b (Å)	10.130(2)	23.4900(15)	11.084(2)
c (Å)	12.087(2)	8.5820(6)	7.9746(17)
α (deg)	66.85(3)	90	90
β (deg)	75.50(3)	106.7310(10)	108.017(4)
γ (deg)	75.23(3)	90	90
V (Å^3)	1000.5(3)	1258.67(14)	890.4(3)
Z	1	2	2
D_{calcd} (g cm^{-3})	2.103	2.556	2.203
λ (Mo Kα), (Å)	0.71703	0.71703	0.71703
T (K)	293(2)	123(2)	273(2)
$2\theta_{max}$ (deg)	56.54	54.98	56.62
abs. coeff, mm^{-1}	8.680	13.576	9.738
# data/params	3070/272	2737/197	2173/123
R; wR for $I > 2\sigma(I)$	0.0323; 0.0588	0.0267; 0.0504	0.0431; 0.0994

Table 2. TGA Decomposition Temperatures

compd	T (°C)
1a	168
1b	167
2a	174
2b	183
3a	176
3b	178

dx.doi.org/10.1021/cm201064c |Chem. Mater. 2011, 23, 4158–4169

Table 3. Summary of PbS Nanoparticle Shapes Obtained from Single-Source Precursors

precursor	reaction conditions	shapes obtained	ref
$Pb[(S_2CNRR')_2]$ $R = C_5H_{11}$, C_6H_{10}, Et, Me, $R' = C_5H_{11}$, C_6H_{10}, $CHMe_2$, C_4H_9	CVD 400−450 °C	granular, platelets, cubic crystallites	41
$Pb[(S_2CNEt_2)_2]$	TOPO + Bi nanoparticles as catalyst 250 °C	nanowires	9b
(2,2′-bipyridyl)$(Pb(SC(O)Ph_2)]$, $[Pb(S_2(PPh_2)_2N)]$	1-thioglycerol, NaOH ∼2 atm, 121 °C	cubes, truncated cubes, rods	16
$Pb(SCH_2Ph)_2$	pyrolysis 150 °C	irregular size	14a
$Pb[S_2P(OR)_2]_2$ $R = C_4H_9$, C_8H_{17}, $C_{12}H_{25}$	oleylamine, n-decane, oleic acid 160 °C	nanocubes	14b
$Pb(SCOPh)_2$	ethylenediamine room temperature	dendrites	18b
$Pb(SCOPh)_2$	oleylamine room temperature	spherical particles	18b
2a, **2b**, **3a**, **3b**	hydrothermal, CTAB, 2 h 170 °C	truncated octahedra	this work
2a, **2b**, **3a**, **3b**	hydrothermal CTAB, 16 h 170 °C	dendritic stars	this work
2a, **2b**, **3a**, **3b**	hydrothermal, CTAB + SDS 160 °C, 16 h	mixture of octahedrons, truncated nanocubes	this work
1a, **1b**, **2a**, **2b**, **3a**, **3b**	solvothermal oleylamine + dodecanethiol 170 °C, 16 h	nanocubes	this work
1a, **1b**, **2a**, **2b**, **3a**, **3b**	solvothermal ethylenediamine 120 °C, 2 h	dendritic stars	this work

and compared the results obtained with those from multiple-source precursors and provide data on the mechanism of growth of NPs.

EXPERIMENTAL SECTION

General. Lead acetate trihydrate (98%), ths (99%), tu (99%), Hpic (99%), H_2dipic (99%), cetyl trimethylammonium bromide (CTAB, technical grade), sodium dodecylsulphonate (SDS), tri*n*-octylamine (TOA; 98%), oleic acid (OA), and 1-dodecanethiol (98%) were obtained from Sigma-Aldrich and H_2sal and ethylenediamine were bought from Fischer Scientific. All the chemicals were used without further purification. All the solvents used for washing and dispersing the precipitated PbS were distilled prior to use employing standard procedures.[19] NMR spectra were recorded on a Bruker Avance-400 MHz NMR spectrometer. Infrared data were recorded on a Nicolet 670 FT-IR spectrometer using attenuated total reflectance. Powder X-ray diffraction (XRD) data were obtained with a Rigaku D/Max-2100PC diffractometer operating with unfiltered Cu Kα radiation (λ = 1.5406 Å) at 40 kV and 40 mA. The contribution from Kα_2 radiation was removed using the Rachinger algorithm. Goniometer alignment was verified by daily analysis of a Rigaku-supplied SiO_2 reference standard. The processing of the powder diffraction results and phase identification was accomplished using the program JADE.[20] TGA studies were performed on a Sieko DT/TGA 200 instrument in an alumina pan under an argon-containing atmosphere. Approximately 20 mg of the sample to be studied was placed in an alumina pan in the furnace of a Sieko TGA/DTA Instruments. The sample was heated to 400 °C at a rate of 10 °C per min. Transmission electron microscope (TEM) experiments were performed by depositing a drop of suspension diluted in hexane on a carbon coated copper grid. The solvent was evaporated and the sample was analyzed using a JEOL 2000FX and JEOL 2010 microscopes that were equipped with energy-dispersive spectrometers (EDS). Conventional and high resolution (HR) TEM imaging, selected area electron diffraction (SAED) and energy dispersive spectroscopy (EDS) methods have been used for the analysis of PbS NPs. Precautions have been taken to prevent structural changes in the studied material caused by heating effects of the electron beam. Scanning electron microscope (SEM) experiments on samples created by depositing a drop of diluted hexane suspension of sample on an aluminum stub. The solvent was evaporated, and the stub was coated with a thin layer of gold in a CRC-150 sputter coater. The sample was then analyzed by an environmental scanning electron microscope, FEI quanta 400 fitted with a field-emission gun. Elemental analyses were performed at the Galbraith Laboratories.

Synthesis of Precursor Molecules. *Synthesis of "$Pb(Hsal)_2(tu)_2$" **1a**.* $Pb(OAc)_2 \cdot 3H_2O$ (379 mg, 1.00 mmol) and H_2sal (276 mg, 2.00 mmol) were dissolved in a 100 mL beaker in 50 mL of water and stirred at reflux until the volume of the solution was reduced to ∼30 mL. tu (160 mg, 2.10 mmol) dissolved in 10 mL of water was added slowly, and the clear solution was stirred for 30 min. The solution was dried under vacuum to isolate white powders of **1a**. It was washed with hexane and dried in a vacuum. Yield ∼300 mg. Melting point ∼110 °C. ^{1}H NMR (DMSO-d^6) 6.84 (m, ArH),7.34 (m, ArH), 7.76 (m, ArH), 4.38 (s, br),^{13}C NMR(DMSO-d^6), 116.52 (ArC), 117.89 (ArC), 118.63 (ArC),130.20 (ArC), 133.45 (ArC), 161.12 (*C*OH), 173.52 (CO_2), 183.75 ($CS(NH_2)_2$). % obsd (% calcd for $Pb(Hsal)_2(tu)_2$), $C_{16}H_{18}PbO_6N_4S_2$: C, 30.77 (30.32); H, 2.60 (2.84).

*Synthesis of "$Pb(Hsal)_2(ths)_3 \bullet 2H_2O$" **1b**.* A similar procedure as described for **1a** was employed, using 184 mg (2.02 mmol) of ths instead of tu. Yield ∼320 mg. Melting point ∼118 °C; ^{1}H NMR (DMSO-d^6), 6.77 (m, ArH),7.27 (m, ArH), 7.76 (m, ArH), 8.1 (m, ArH), 4.03 (m, br),^{13}C NMR (DMSO-d^6), 116.55 (ArC), 117.90 (ArC), 119.48 (ArC), 130.24(ArC), 133.34 (ArC), 161.03(*C*OH), 174.06(CO_2), 181.05 ($CSNH_2NHNH_2$). % obsd (% calcd for $Pb(Hsal)_2(ths)_3 \cdot 3H_2O$), $C_{17}H_{31}PbO_9N_9S_3$: C, 24.42 (25.24); H, 3.73 (3.86).

*Synthesis of "$Pb(pic)_2(tu)$" **2a**.* An aqueous solution (100 mL) of $Pb(OAc)_2 \cdot 3H_2O$ (379 mg, 1.00 mmol) and Hpic (246 mg, 2.00 mmol) was stirred at 100 °C in a beaker until the volume of the solution was reduced to ∼60 mL. An aqueous solution of tu (154 mg, 2.02 mmol) was added and the resulting clear solution was dried under a vacuum. The product was washed with diethyl ether.^{1}H NMR (DMSO-d^6), 7.06 (s, broad, H of thiourea), 7.15 (m, ArH), 7.70 (m, ArH), 8.00 (m, ArH), 8.77 (m, ArH) ^{13}C^{15} NMR (DMSO-d^6), 125.91 (ArC), 126.51 (ArC), 139.18 (ArC), 133.25 (ArC), 146.96 (ArC), 151.92 (*C*COOH), 169.74 (CO_2) 183.76 ($CS(NH_2)_2$). % obsd (% calcd) for $C_{13}H_{12}PbO_4N_4S$: C, 29.47 (29.60); H, 2.19 (2.29).

*Synthesis of "$[Pb(pic)_2(ths)_2]_2$," **2b**.* $Pb(OAc)_2 \cdot 3H_2O$ (379 mg, 1.00 mmol) and Hpic (246 mg, 2.00 mmol) were dissolved in 200 mL of water and the resulting solution was stirred at 100 °C in a beaker until the volume of the solution was reduced to ∼10 mL. Solid ths (184 mg, 2.02 mmol) was added to the hot solution of lead(II) picolinate and the resulting clear solution was left to cool for 2 days to yield colorless crystals. Yield: 470 mg. Melting point: ∼178 °C. ^{1}H NMR (DMSO d^6), 7.06 (s, broad, H of tu), 7.15 (m, ArH), 7.70 (m, ArH), 8.00 (m, ArH), 8.77(m, ArH) ^{13}C NMR (DMSO-d^6), 125.95 (ArC), 126.45 (ArC),

dx.doi.org/10.1021/cm201064c |*Chem. Mater.* 2011, 23, 4158–4169

139.22(ArC), 146.74 (ArC), 151.87 (CCOOH), 169.49 (CO_2) 181.14 ($CSNH_2NHNH_2$). % obsd (% calcd for $Pb(pic)_2(ths)_2$) $C_{14}H_{18}PbO_4N_8S_2$: C, 26.00 (26.53); H, 2.97 (2.86).

Synthesis of [Pb(dipic)(tu)(H$_2$O)]$_2$·2H$_2$O, ***3a***. $Pb(OAc)_2 \cdot 3H_2O$ (279.00 mg, 1.00 mmol) was dissolved in 20 mL water, and then 20 mL of an aqueous solution of H_2dipic (415 mg, 2.00 mmol) was added. The mixture was allowed to stir resulting in the precipitation of some white Pb(dipic). The solution was filtered and an aqueous solution of tu (154 mg, 2.02 mmol) was added to the filtrate. The resulting solution was stirred overnight and left for crystallization. After 48 h, a microcrystalline white precipitate formed, which was washed with water and hexane and then dried in vacuum to yield 256 mg of **3a**. In an alternative method, a solution containing $Pb(NO_3)_2$ and thiourea was layered with a solution of Na_2(dipic) and thiourea and allowed to stand for several days. Very nicely shaped prismatic crystals resulted. ^{1}H NMR (DMSO-d^6) 8.233 (m,ArH), 7.6 (br, m, H of th), ^{13}C (DMSO-d^6) 165.49(CO2), 149.22(CCOOH), 141.69(ArC), 125.33(ArC), 181.66-($CS(NH_2)_2$). Elem. anal.: %obsd (%calcd for $[Pb(dipic)(tu)(H_2O)]_2 \cdot 2H_2O$, $C_{16}H_{22}Pb_2S_2N_6O_{12}$: C, 20.02, 19.70 (19.83); H, 2.08. 2.32 (2.29); N, 8.60 (8.67).

Synthesis of [Pb(dipic)(ths)$_2$]·2H$_2$O, ***3b***. A similar method to the first procedure described for **3a** was employed using 184 mg (2.02 mmol) of ths instead of tu. Yield: 350 mg. Melting point: 134 °C. ^{1}H NMR (DMSO-d^6) 8.645(s, ArH), 8.162(s, ArH), 7.194(br, m, H of ths) ^{13}C (DMSO-d^6), 148.86(CCOOH), 140.23(ArC), 127.24 (ArC), 181.02 ($CSNH_2NHNH_2$). % obsd (% calcd for $[Pb(dipic)(ths)_2] \cdot 2H_2O$) for $C_9H_{15}PbO_5N_6S_2$: C, 14.84 (18.30); H, 2.92 (2.90). Repeated attempts to obtain satisfactory elemental analyses were not successful, presumably because of the competing coformation of insoluble polymeric lead dipicolinate complexes.

Single-Crystal X-ray Structural Determinations. The data for **2b**, **3a**, and **3b** were collected at 298, 123, and 273 K, respectively, on a Bruker SMART 1000 CCD diffractometer equipped with a Mo-target X-ray tube in a hemisphere with 10 or 15 s exposure times.[21] The frames were integrated with the Bruker SAINT software package[22] and corrected for absorption effects using empirical methods (SADABS).[23] X-ray crystallographic data collection and refinement parameters are given in Table 1. The structures were solved using direct methods and refined by full-matrix least-squares on F^2 using the Bruker SHELXL software package.[24] The coordinates of lead and sulfur atoms were found using direct methods. The remaining atoms were located in subsequent least-squares difference Fourier cycles. Hydrogen atoms were included in idealized positions. Anisotropic displacement parameters were assigned to all non-hydrogen atoms.

Synthesis of Nanocrystals from Single-Source Precursors (SSPs). *(i). Aqueous Media. Decomposition of the Precursors in the Presence of CTAB.* In a typical procedure for the synthesis of PbS nanoparticles by hydrothermal decomposition, 0.10 g of the precursor was placed in a ~23 mL Teflon-lined stainless autoclave to which 20 mL of distilled water and 0.05 g of CTAB was added. The autoclave was sealed and maintained at 160 °C for 2 h. The reaction was then quenched by immersing the autoclave in liquid N_2 for 15 min. The black precipitate was collected by centrifugation after the addition of ethanol. The product was washed repeatedly with ethanol and redispersed in hexane. This same procedure was repeated changing the time intervals to 5 and 16 h.

Decomposition of the Precursors in an Aqueous Mixture of SDS and CTAB. Approximately 0.10 g of the precursor was placed in a ~23 mL Teflon-lined stainless autoclave. To this was added 20 mL of distilled water, 0.025 g of CTAB, and 0.025 g SDS. The autoclave was sealed and maintained at 160 °C for 16 h. The reaction was quenched as described above. The black precipitate was collected by addition of ethanol and centrifugation. It was washed repeatedly with ethanol and redispersed in hexane.

(ii). Nonaqueous Media. Decomposition in the Presence of OA and Dodecanethiol. The appropriate precursor (0.10 g) was mixed with 8 mL of OA and stirred for 30 min. To this mixture was added 1 mL of dodecanethiol and the resulting solution was stirred for 10 min. The mixture was heated in Teflon lined stainless steel autoclave for 16 h at 170 °C. It was then allowed to cool to room temperature. The black precipitate was collected by addition of ethanol and centrifugation. It was washed repeatedly with ethanol and redispersed in hexane.

Decomposition in the Presence of OA and TOA. The appropriate precursor (0.10 g) was mixed with 10 mL of TOA and 2 mL of OA in a three-neck flask fitted with a reflux condenser under a constant flow of argon. Prior to mixing, the OA and the TOA were dried for 30 min under vacuum at 70 °C. The resulting mixture was heated at 120 °C for 1 h. An aliquot was collected from the solution after it cooled to room temperature. The solid was collected upon addition of ethanol and centrifugation. It was washed with ethanol repeatedly and redispersed in hexane.

Decomposition in the Presence of Ethylenediamine. The appropriate precursor (0.10 g) was mixed with 8 mL of ethylenediamine and stirred for 30 min. The mixture was heated in Teflon-lined stainless steel autoclave for 2 h at 120 °C. It was then allowed to cool to room temperature. The black precipitate was collected by addition of ethanol and centrifugation. It was washed repeatedly with ethanol and redispersed in hexane.

Synthesis of Nanocrystals from Multiple-Source Precursors (MSP). *Aqueous Media. Decomposition in the Presence of CTAB and H$_2$sal, Hpic, or H$_2$dipic.* In this set of reactions, $Pb(OAc)_2 \cdot 3H_2O$ and tu or ths were decomposed in presence of free aromatic acids H_2sal, Hpic or H_2dipic using CTAB as surfactant. For H_2sal, Hpic, the molar ratio of the reagents were 1:2:2 for $Pb(OAc)_2 \cdot 3H_2O$: (tu or ths): acid, respectively, whereas for H_2dipic, it was 1:2:1. In a typical procedure, 0.5 mmol (0.19 g) of $Pb(OAc)_2 \cdot 3H_2O$ and 0.076 g (1.0 mmol) of tu were put in a stainless autoclave, to which 1.0 mmol of the carboxylic acid was added followed by a solution of 0.20 g CTAB in 20 mL distilled water. The autoclave was sealed and maintained at 170 °C for 16 h. The reaction was quenched by immersing the autoclave in liquid N_2 for 15 min. The black precipitate was collected by addition of ethanol and centrifugation. It was washed repeatedly with ethanol and redispersed in hexane.

Nonaqueous Media. Decompositions in the Presence of OA and Dodecanethiol. In this set of reactions 0.19 g (0.50 mmol) of $Pb(OAc)_2 \cdot 3H_2O$ and 0.076 g (1.0 mmol) of tu or 0.091 g (1.0 mmol) of ths were mixed with 8 mL of OA and stirred for 30 min. To this mixture was added 1 mL of dodecanethiol and the resulting solution was stirred for an additional 10 min. The mixture was heated in Teflon lined stainless steel autoclave for 16 h at 170 °C. It was then allowed to cool to room temperature. The black precipitate was collected by addition of ethanol and centrifugation. It was washed repeatedly with ethanol and redispersed in hexane.

Decomposition in the Presence of OA. These reactions were carried out in a three-neck flask fitted with a reflux condenser. Commercially available OA was dried by heating 5 mL of the acid with 1 mL of acetic anhydride at 70 °C for 30 min followed by drying under vacuum at 120 °C for 30 min. Next 0.38 g (1.0 mmol) of $Pb(OAc)_2 \cdot 3H_2O$ was added to the dry OA and stirred at 50 °C for 30 min to convert it into $Pb(oleate)_2$. The resulting solution was then dried under vacuum for 30 min at 120 °C to remove the acetic acid produced in the course of reaction. To this mixture dry tu (0.076 g) was added directly under the flow of argon and the reaction mixture was heated. Solution changed color to black at 120 °C. An aliquot was collected 10 min after it changed color. The black precipitate was collected upon addition of ethanol and centrifugation. It was washed repeatedly with ethanol and redispersed in hexane.

Decomposition in the Presence of OA and TOA. This set of reactions was carried out in a three-necked flask fitted with a reflux

Scheme 1. Synthetic Summary of the Lead tu and ths Complexes

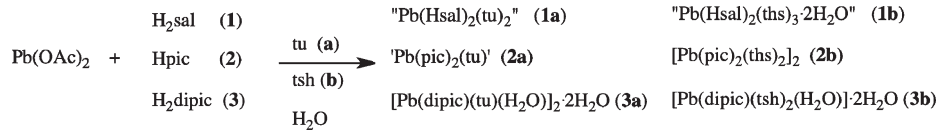

condenser. Five milliliters of OA was dried by heating with 1 mL of acetic anhydride as described above. $Pb(OAc)_2 \cdot 3H_2O$ (0.38 g) was added and treated as described above to convert it into $Pb(oleate)_2$. To this mixture 0.076 g (1.0 mmol) tu in 6 mL TOA was added under a flow of argon and the resulting mixture was heated at 170 °C. An aliquot was collected from the reaction 10 min after the solution turned black. The solid was collected upon addition of ethanol and centrifugation. It was washed with ethanol repeatedly and redispersed in hexane.

RESULTS AND DISCUSSION

Syntheses and Structures of the Molecular Precursors. New single-source molecular precursors for PbS have been prepared by mixing aqueous solutions of lead acetate trihydrate with the appropriate aromatic carboxylic acid followed by addition of thiourea (tu) or thiosemicarbazide (ths), as highlighted in Scheme 1. It was found that the ability to crystallize the compounds was greatly affected by their solubility and the state of dynamic equilibrium between the free and coordinated ligands in the solvent. The lead dipicolinate derivatives were found to be least soluble among the three, and the syntheses were complicated by formation of the neutral coordination polymer $[Pb(dipic)]_n$.[25] The formation of $[Pb(dipic)]_n$ as a side product explains the low yields of the dipicolinate precursors as compared to the other four. In the case of **3b**, the addition of a slight excess of ths was necessary to produce well-formed crystals. It is believed that the extra ths assisted in shifting the equilibrium toward formation of **3b**. An alternate synthesis of the $dipic^{2-}$ compounds in which a solution containing the sodium dipicolinate and tu or ths was allowed to diffuse in slowly to a solution containing a Pb^{2+} salt and either tu or ths helped to overcome the difficulties in obtaining nicely crystalline material that was free of the insoluble $[Pb(dipic)]_n$.

The $Hsal^-$ complexes were found to be the most soluble followed by the pic^- and then $dipic^{2-}$ derivatives, consequently we have not yet been successful in crystallizing these compounds in a form suitable for single crystal X-ray diffraction analysis and their composition is tentative. For **1a**, the elemental analyses agree reasonably well with the formulation $Pb(Hsal)_2(tu)_2$ and this composition is analogous to that observed for the Cd^{2+} analogue.[14c] In contrast, the closest formulation to the observed experimental analyses for **1b** was a compound having three ths molecules per Pb^{2+} ion. Indeed, electrospray mass spectroscopy of this compound in solution allowed the detection of several species, including $Pb(sal)(ths)_3^+$, $Pb(sal)^+$, and $Pb(ths)_2^+$; however, only one set of ^{13}C NMR signals for the salicylate ligands was observed suggesting a dynamic equilibrium in solution and possibly the reversible dissociation of the ths ligands. In the ^{13}C NMR spectra of all of the compounds, the chemical shift difference between the ^1H signals of the free and coordinated ligands was small making analysis difficult. Dynamic equilibrium and the existence of a mixture of species in solution could also explain why all the attempts to crystallize the salicylate complexes were unsuccessful. We were also not successful in obtaining single crystals of **2a**, the $Pb(pic)_2$ derivative with tu; however, the elemental analyses were consistent with a formulation of $Pb(pic)_2(tu)$. Although it might be expected that this compound would be similar to **2b** which has two ths ligands bound per Pb^{2+}, the $dipic^{2-}$ derivatives show a similar situation; **3a** shows only one tu bound to Pb^{2+} ion, whereas in **3b** two ths ligands are attached. In contrast, complexes **2b, 3a** and **3b** produced crystals suitable for single crystal X-ray diffraction studies. A summary of selected data acquisition and refinement parameters is given in Table 1, whereas selected bond distances and angles for the three compounds are found in Tables S1 and S2 in the Supporting Information.

The Pb^{2+} ion in compound **2b** is coordinated by two bidentate picolinate ligands and two monodentate ths molecules with the donor atoms in a highly distorted coordination environment (Figure 1). Each picolinate ion acts as a bidentate ligand coordinating to the central Pb(II) by both the pyridyl N and one carboxylate O atom, and each ths moiety acts as a monodentate ligand coordinating through the S atom. Furthermore, these units are arranged into weak dimers through the mutual bridging of one of the carboxylate oxygen atoms of one pic^- ligand to the Pb^{2+} ion of an adjacent molecule. A similar compound was observed for Cd^{2+}, $[Cd(pic)_2(ths)_2] \cdot 2H_2O$;[24] however, there the Cd^{2+} ion is six-coordinate with no dimer formation. The Pb−N bond distances of **2b** are short (2.560(5), 2.620(5) Å compared to those in $Pb(H_2tpaa)Cl$ (H_2tpaa = α,α',α''-nitrilotri(6-methyl-2-pyridinecarboxylic acid)): 2.645(6) (chelating) and 2.720(6), 2.803(6) Å (nonchelating)).[33] Furthermore, these dimeric units are linked into weak ladder polymers by bridging tu ligands with Pb···S interactions at 3.450(2) Å, which can be considered as secondary bonds (Figure 1C). Additional weak interactions include inter- and intramolecular N−H···O hydrogen bonds and $\pi-\pi$ stacking between the N1−C12−C13−C14−C15−C16 aromatic groups (centroid-to-centroid distance = 3.688(6) Å and interatomic contacts ranging from 3.675(6) to 3.706(6) Å).

The crystal structure of **3a** also consists of centrosymmetric dimeric molecules (Figure 2). Each Pb^{2+} ion is coordinated by two carboxylate oxygen atoms and one pyridyl nitrogen atom from one $dipic^{2-}$ ion in addition to a carboxylate oxygen from a $dipic^{2-}$ attached to an adjacent Pb^{2+} ion producing dimeric units. A water molecule and a tu complete the coordination sphere of each Pb^{2+}, giving rise to a hemidirected pentagonal pyramidal mode with the tu S atom in the apical position. The bridging carboxylate group C11−O11−O12 displays a monatomic bidentate coordination mode: $\kappa^0{:}\kappa^2{:}\mu_2$. In contrast, three types of bridging carboxylate groups were found in the structure of a Bi(III) dipicolinate-thiourea complex $[Bi_6(dipic)_8(Hdipic)_2(tu)_8]$: $\kappa^0{:}\kappa^2{:}\mu_2$, $\kappa^1{:}\kappa^1{:}\mu_2$ and $\kappa^1{:}\kappa^2{:}\mu_2$,[25] whereas a Cd(II) analogue, $[Cd(dipic)(tu)_2]$, has no bridging carboxylate groups.[24] The Pb−N and Pb−O bond distances in **3a** were compared with other Pb salts of pyridine dicarboxylic acids (H_2pdca).[32] For **3a**, Pb−O distances are found to be 2.461(3) and 2.563(3) Å. Pb−O distances from other molecules include 2.480(4) in Pb(2,3-pdca), 2.445(10) in Pb(2,4-pdca)·H_2O, and

dx.doi.org/10.1021/cm201064c |Chem. Mater. 2011, 23, 4158–4169

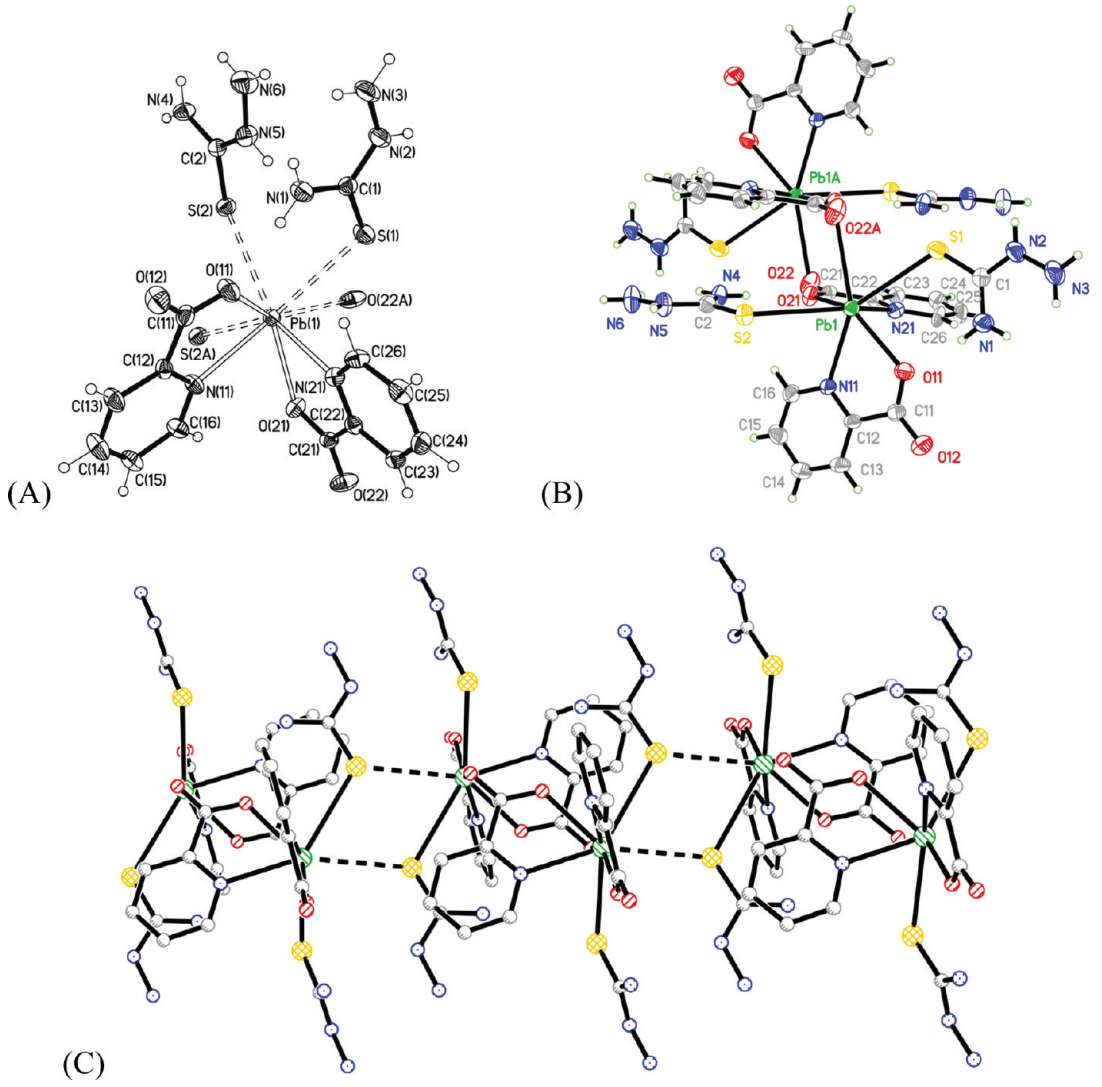

Figure 1. X-ray structure: (A) Monomeric subunit of compound **2b** with thermal ellipsoids at 40% probability level. (B) Dimeric unit of **2b** formed via dipicolinate bridges. (C) Ladder polymer formed by weak briding dimeric units via additional Pb···tu interactions.

2.445(4) Å in Pb(2,5-Hpdca)$_2$·2H$_2$O. The longer Pb−O distance in **3a** is likely a result of its involvement in as a bridging ligand. The Pb−N bond distance in **3a** is 2.491(3) Å and lies within the range seen for other molecules: 2.535(4) Å in Pb(2,3-pdca)), 2.391(9) Å in Pb(2,4-pdca)·H$_2$O), and 2.448(4) Å in Pb(2,5-Hpdca)$_2$·2H$_2$O. The Pb−S bond at 2.7389(14) Å was shorter than that found in literature precedents: 3.0410(8) and 3.0987(8) Å) in PbCl$_2$(tu)$_2$ and 3.0812(4) Å in PbBr$_2$(tu).[34,35] The Pb−O(1) and Pb(O11a) bonds (2.758(4) and 2.789(3) Å) are longer than the other two Pb−O$_{carboxylate}$ bonds and can be considered as secondary. In the crystal packing of **3a** the parallel polymer chains are linked by hydrogen bond interactions involving the carboxylate groups, tu ligands, and water molecules (Figure 2C).

In **3b** (Figure 3) the central Pb^{2+} ion is coordinated with two carboxylate oxygen atoms and one pyridyl nitrogen atom of the dipic^{2-} ligand and the sulfur atoms of two ths ligands. The coordination environment of the Pb(II) atom is highly distorted. The Pb−O bond distances are significantly shorter (2.436(8) Å) than those found in Pb(2,4-pdca)·H$_2$O, Pb(2,5-Hpdca)$_2$·2H$_2$O, and Pb(2,3-pdca), whereas the Pb−N bond (2.466(15) Å) is well within the range reported for those molecules. The ths molecules act as S-bridging ligands and bind adjacent Pb^{2+} ions into one-dimensional ladder polymeric chains through Pb−S secondary interactions at 3.487(4) Å (Figure 3b). These interactions give the Pb^{2+} ion a coordination number of six. The N atoms of the ths ligands are not involved in coordination. In contrast, the ths ligand in $\{[Bi_2(dipic)_3(ths)(H_2O)_2]\cdot H_2O\}_\infty$ is N,S chelating and the polymeric chain structure is generated by bridging $\kappa^1{:}\kappa^2{:}\mu_2$ carboxylate groups.[25] Interestingly enough, the structure of the Cd^{2+} analogue [Cd(dipic)(ths)$_2$(H$_2$O)]·2H$_2$O is monomeric and contains both S-bound monodentate and N,S-chelate ths ligands.[24] The central Pb(II) in **3b** is only pentacoordinate, whereas in the Cd^{2+} analogue the central Cd^{2+} ion is seven-coordinate. The polymeric chains in **3b** are linked further into a supramolecular structure through an extended hydrogen bonding network that involves the lattice water molecule, a carboxylate oxygen of a dipic^{2-} ligand and two different ths ligands. As in compound **3a**, no $\pi-\pi$ stacking interactions between the aromatic groups of the dipic^{2-} ligands were detected.

Conversion of the Precursors to PbS. We have been exploring the effect of single source molecular precursors on morphology and size in nanoparticle synthesis.[3a,14c,14e,26] The

dx.doi.org/10.1021/cm201064c |*Chem. Mater.* 2011, 23, 4158–4169

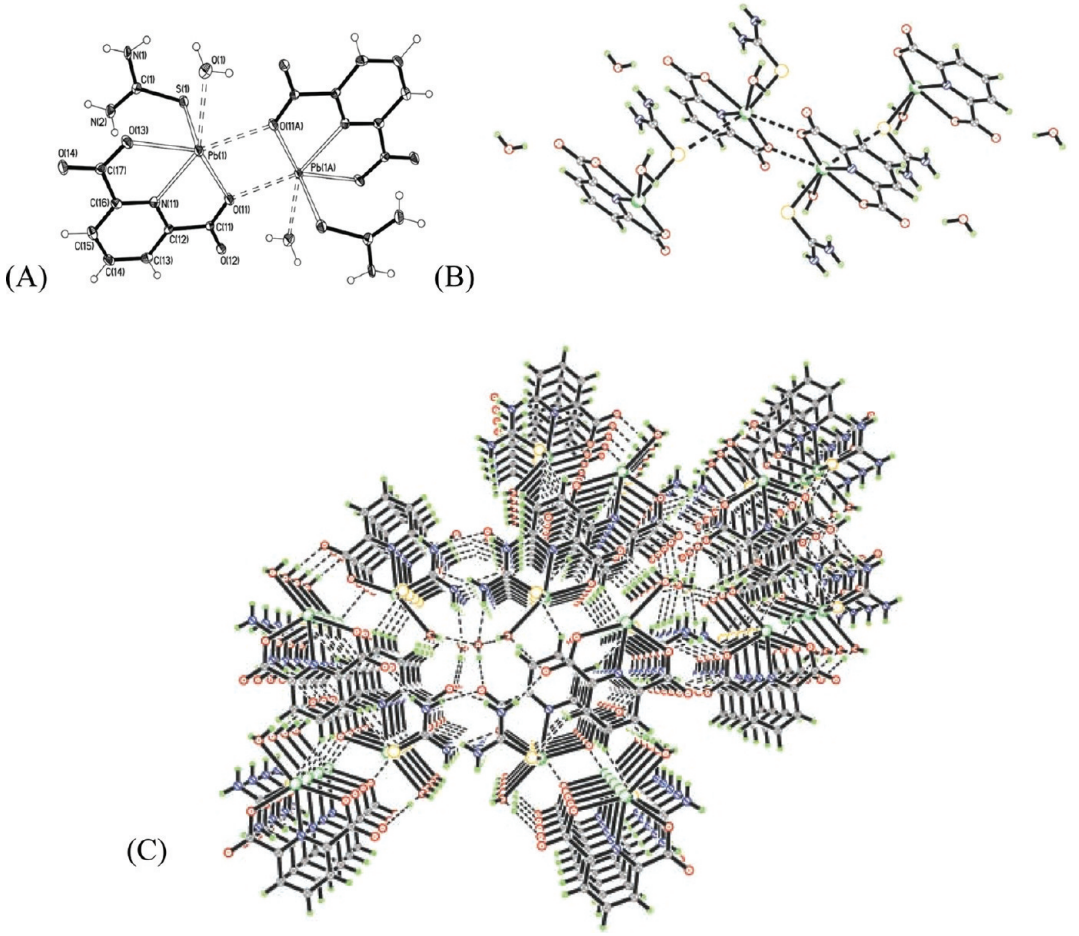

Figure 2. X-ray structure: (A) Cosely associated dimer **3a** with thermal ellipsoids at 50% probability level. The lattice water molecules were omitted for clarity. (B) Extended view of the dimer showing addition intermolecular Pb···tu interactions. (C) Packing diagram of **3a** showing channels filled with the lattice water molecules and their H-bonding contacts.

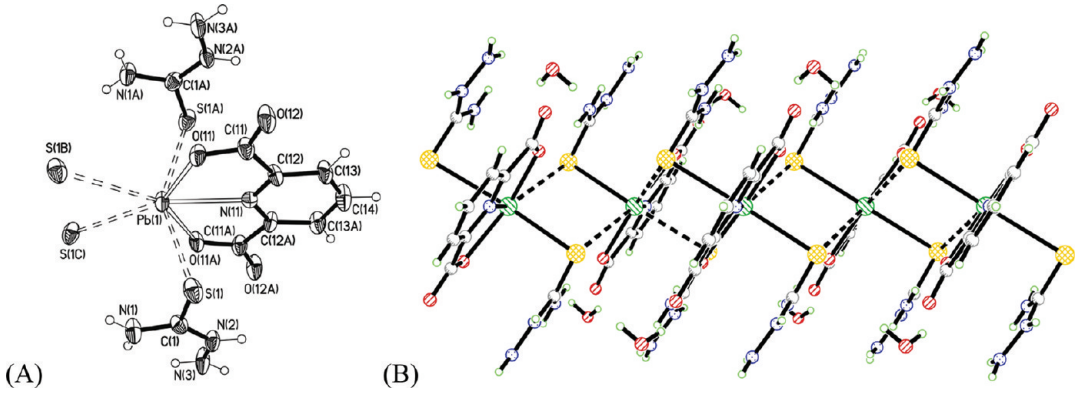

Figure 3. X-ray structure of (A) the asymmetric unit of **3b** with thermal ellipsoids at 40% probability level. (B) One-dimensional ladder polymer **3b** formed by briding tu ligands.

use of a single-source precursor can help control the metal stoichiometry in the final product, similar to complexes used for MOCVD.[26a,27] As mentioned above, molecular precursors also help achieve a homogeneous distribution of metal ions in the final product as a result of the intimate mixing in the molecular level and can impart unusual or desirable structural features in the end product.[11−15] Presumably in cases where multiple source precursors have been used, prior coordination of the sulfur-containing compound to the lead ion occurs in such a fashion to promote decomposition of the ligand and formation of lead-bound sulfide. The use of single-source precursors may thus have an advantage in assembling the necessary components into a single molecule facilitating and tuning nanoparticle growth kinetics.

dx.doi.org/10.1021/cm201064c |*Chem. Mater.* 2011, 23, 4158–4169

Decomposition of Precursors. Bulk decompositions of the precursors were followed by thermogravimetric analysis (TGA). All of the precursors undergo a single decomposition step around 170 °C, giving rise to pure crystalline galena PbS as the end product. The decomposition temperature of the precursors is listed in Table 2 and the TGA traces are given in the Supporting Information. On the basis of the TGA results it is reasonable to conclude that during the single large decomposition step the organic residue of the single-source precursor is removed leaving behind pure PbS. Based on the TGA results, the solution decomposition reactions were conducted at 170 °C using a variety of surfactants. The morphologies and structures of the solution decomposition products were examined by SEM and TEM.

Traditionally anisotropic shaping in a nanocrystal has been observed under a variety of conditions: (1) seed-mediated growth is often observed in the vapor−liquid−solid (VLS) or solution−liquid−solid (SLS) processes where nanocrystal seeds facilitate shaping;[9b,28] (2) oriented attachment resulting from sharing of high energy faces of adjacent crystals to reduce surface energy and attain thermodynamic stability as has been reported in several different systems such as PbSe, ZnS, CdTe, etc;[13,29] (3) growth of the nanocrystals on a template such as a polymer substrate;[6] (4) selective binding of surfactants to specific crystalline facets. The latter results in stabilization of those facets over others and thus different growth rates are induced to different facets, thus leading to anisotropy. We, along with several other groups, have observed this in our study of CdS, Bi_2S_3 and other systems.[14c,26b,30] Although faceted growth mediated by selective adhesion by surfactants plays a role, we and others[2] have demonstrated that crystal shaping could be manipulated by repeated cycles of growth and dissolution.[26a]

Faceted Growth and Dissolution Growth in Aqueous Media Starting from Single-Source Precursors. The cycling between faceted and dissolution growth in aqueous media depends on several growth parameters such as temperature, time, concentration and type of surfactants. To monitor the growth of particles (faceting/dissolution) with time the reaction was quenched at intervals of 1, 2, 5, 8, and 16 h. The reactions were carried out in stainless-steel lined Teflon vessel maintained at 170 °C in the hydrothermal oven. In Figure 4, SEM images are shown for (A) 2 h, (B, C) 5 h and (D) 16 h.

In the early stages (2 h) of the decomposition faceted growth leading to the formation of cuboctahedral micrometer-sized crystals terminated by low index planes predominates. In this growth regime the relative growth ratio (R) of the {100} and {111} faces determines the final morphology. The surface energies associated with different crystallographic planes are usually different and a general sequence can be elucidated as {111} < {100} < {110}.[31] As shown by others, when R is 1.73, an octahedron is formed that is bounded by {111} faces, whereas when R is 0.58 a cube bound by {100} faces results.[32] However for the particles with 0.58 < R < 1.73 both {100} and {111} faces are present. In Figure 4A, the truncated octahedra obtained in the presence of CTAB after 2 h of reaction time have six square {100} faces and eight hexagonal {111} faces. The polar $-NMe_3^+$ headgroup of CTAB stabilizes charged faces.[33]

When the reaction time is extended to 5 h a dissolution growth mediated by Ostwald ripening takes over leading to the incorporation of the octahedral seed into large dendritic crystals. The initial octahedral seeds appear to have dissolved completely and transformed into large leaflike dendritic crystals. These dendritic structures are very stable at this stage. Nearly identical dendritic

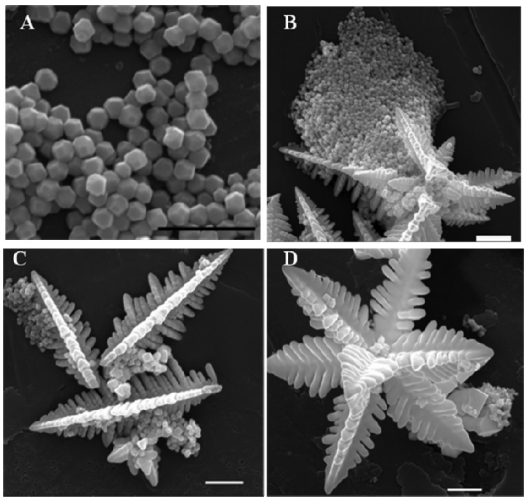

Figure 4. SEM images of PbS nanoparticles synthesized from precursor **2b** by using aqueous CTAB: (A) 2, (B, C) 5, and (D) 16 h. All scale bars = 1 μm.

shapes as those seen in Figures 4D and 8B were observed for PbS previously and the orientation of the arms along the ⟨111⟩ directions was confirmed.[18b,34]

To probe the role of surfactant we carried out the reaction using an equimolar mixture of CTAB and SDS. We chose SDS as its sulfonate group (SO_3^-) is expected to create stronger bonds with Pb^{2+} compared to CTAB's $R-S^-$ and $-^+NMe_3$ interactions, but SDS is also a polar surfactant that adsorbs preferentially to the polar {111} faces similar to CTAB. Thus the presence of SDS in the reaction mixture is expected to effectively lower the energy of {111} as previously reported.[34] In addition to the stabilization of the {111} faces, when a mixture of SDS and CTAB was used, considerable ripening occurred as indicated by a heterogeneous mixture dominated by hexa-branched structures in addition to nanocubes and nanooctahedra with slightly truncated or rounded edges (Figure 5). Similar star shapes, which appear to be octahedral particles lying on a face, have been observed in the decomposition of $Pb(OAc)_2$ in the presence of ethylene glycol.[35] The points in these particles were determined to be pointing in the ⟨100⟩ directions. The use of cetyl trimethylammonium bromide (CTAB), dodecyltrimethylammonium bromide (DTAB) or sodium dodecylsulphonate (SDS) morphology tuning of PbS has been achieved to synthesize nanocubes, hexagons, octahedra and dendritic stars in a controlled manner.[4] The TEM image for a large star-shaped particle from our system is shown in Figure 5(C) is oriented along the [111] zone axis, corresponding to the SAED pattern in Figure 5(D), with the growth direction being in the ⟨100⟩ directions similar to that reported by Zhao et al.[35]

Faceted Growth and Dissolution Growth in Nonaqueous Media Using Single-Source Precursors. When the decomposition reactions were carried out in oleylamine with added dodecanethiol, nanocubes were obtained (Figure 6, Figure S11 in the Supporting Information). The nanocubes are oriented along the ⟨001⟩ zone axis as anticipated and show the SAED pattern typical of the cubic rock salt structure. Previous reports on the growth mechanism of PbSe nanocrystals discuss the effect of OA.[29b] The driving force in formation of the cubes lies in higher growth rate along ⟨111⟩ as compared to ⟨100⟩. OA is relatively nonpolar and nonselective, binding to both {100} and {111} faces. Because the intrinsic surface

dx.doi.org/10.1021/cm201064c |*Chem. Mater.* 2011, 23, 4158–4169

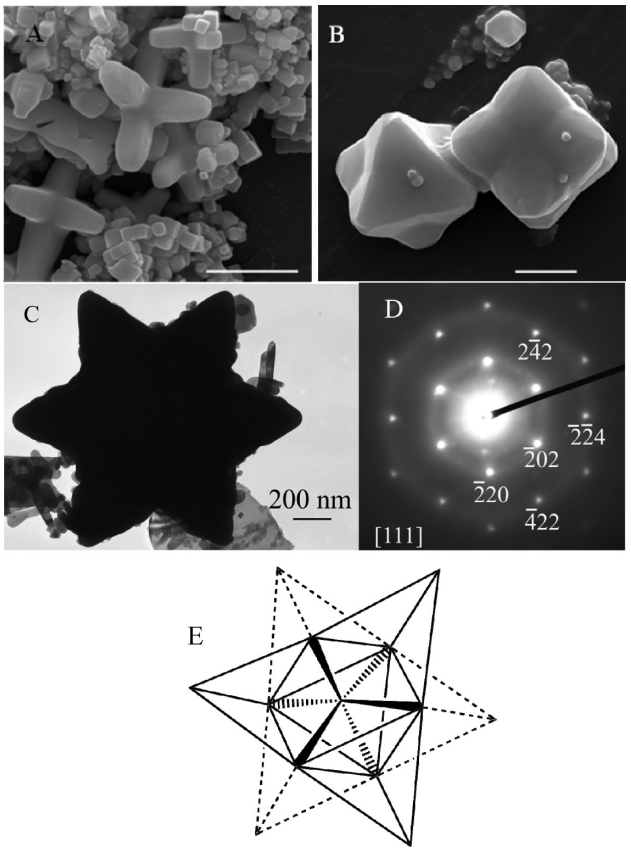

Figure 5. (A, B) SEM images of PbS nanoparticles generated with equimolar aqueous mixture of CTAB and SDS from precursor **2b**. (A) Generalized view of bulk mixture of microstructures produced in the decomposition. (B) Closer look at the octahedral and tetracubic structures. The scale bars in the SEM images represent 1 μm. (C) Bright-field (BF) TEM image of a star-shaped particle. (D) SAED pattern from the particle in C. (E) Line drawing showing the two-dimensional projection of an octahedral crystal as in (C). The thickness of this particle prevents the observation of thickness contrast as observed for the similar particles reported elsewhere.[35].

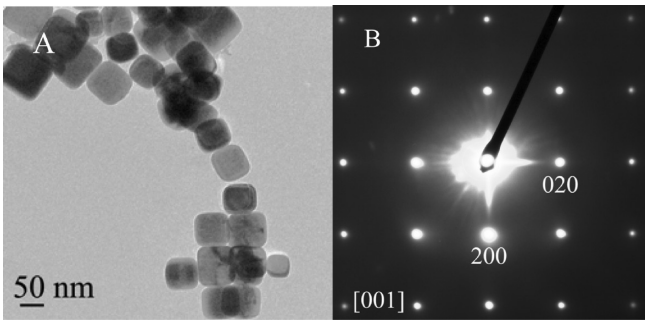

Figure 6. (A) BF TEM image of representative nanocubes generated in oleylamine and dodecanethiol from precursor **2a**. Similar structures were observed for the other precursors under similar conditions (see Figure S11). (B) SAED pattern from one of these particles showing that the nanoparticles are oriented along the [001] zone axis.

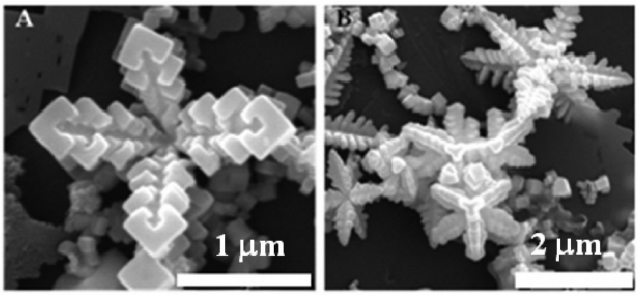

Figure 7. SEM images of dendritic nanostars and interwined quasi-cubic structures generated by decomposition in ethylenediamine using (A) **2a**, (B) **1b**.

energy of the {111} faces is more than that of {100}, growth takes place along {111} giving rise to a cubic nanocrystal from a tetradecahedral seed. It has been shown by Cheon et al. that the presence of dodecanethiol molecules in the reaction mixture has different effect.[36] Dodecanethiol tends to bind to the {111} faces via a μ_3-bonding mode, thus lowering the energy of the {111} faces as compared to {100}. An increase in the amount of dodecanethiol tends to produce truncated cubes and ultimately truncated octahedra. We found a similar observation for increasing amounts of dodecanethiol (see the Supporting Information).

When the decomposition reactions were carried out in presence of a short chain amine such as ethylenediamine, a mixture of dendritic structures along with some interlinked quasi-cube shaped nanocrystals was obtained (Figure 7). At a reaction temperature of 120 °C in the presence of ethylenediamine, the oscillatory growth between the faceted growth and dissolution growth is observed. The growth mechanism of dendritic and star-shaped PbS nanoparticles has been investigated and reported.[4,5,35] However, we identified an interesting growth regime (Figure 7A) that oscillates between faceting and dissolution growth leading to a regular nanoarchitecture at extended length scale. This concept is very important for the synthesis of nanomaterials at extended length scale where self-assembly is not satisfactory.[37]

The hypothesis of growth via oriented attachment[29b,38] was excluded as we analyzed the sample using high-resolution (HR) TEM and found no epitaxial connection between the building block's facets consistent with the oriented attachment growth mechanism. The presence of lateral etching mark and the platelike shape of the building blocks indicate a complex growth mechanism in which supersaturation oscillates between 2D and 3D growth. A similar phenomenon has been observed previously in Mn(II) oxide system,[3a] as well as in other systems.[39]

Faceted Growth and Dissolution Growth in Aqueous and Nonaqueous Media Using Multiple Source Precursors (MSP). We have also investigated the faceted and dissolution growth using multiple sources precursors. However, the reproduction of the shapes previously observed required slight modification of reaction conditions. Table 4 provides a summary and comparison of results obtained from SSP and MSP under similar reaction conditions. When $Pb(OAc)_2 \cdot 3H_2O$ and tu or ths was heated in presence of CTAB and H_2sal, Hpic or H_2dipic, dendritic stars formed (Figure 8). These reactions took considerably less time than their SSP counterparts, which can be rationalized by the slower rate of solvolysis of the SSPs owing to the strong binding of the chelating ligands. Reactions in presence of an equimolar mixture of CTAB and SDS gave rise to mostly irregular shaped particles with some cubes (see Figure S13 in the Supporting

dx.doi.org/10.1021/cm201064c |*Chem. Mater.* 2011, 23, 4158–4169

Table 4. Summary and Comparison of NP Shapes Obtained from Single- and Multiple-Source Precursors under Similar Reaction Conditions

reaction conditions	single source precursors	multiple source precursors
hydrothermal reaction with CTAB	dendritic stars	dendritic stars (in presence of free acid in reaction mixture)
hydrothermal reaction surfactant mixture of CTAB + SDS	mixture of octahedra, six-armed stars, truncated nanocubes	interlinked cubes and irregular shaped particles
hydrothermal reaction with oleylamine and dodecanethiol	nanocubes	mixture of nanocubes and octahedra
hydrothermal reaction with ethylenediamine	dendritic stars	mixture of cubes and some irregular shapes with a few dendritic stars
reflux in oleic acid	no decomposition	mixture of nanorods and nanocubes
reflux in a mixture of oleic acid and trioctylamine	irregularly shaped and sized particles	mixture of split-end rods and nanocubes

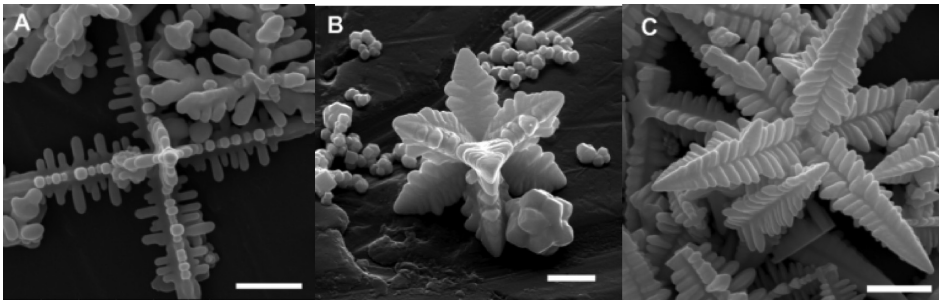

Figure 8. SEM images of PbS dendrites synthesized from MSP by using CTAB as surfactant: (A) decomposition of $Pb(OAc)_2 \cdot 3H_2O$ and ths in presence of free H_2sal; (B) decomposition of $Pb(OAc)_2 \cdot 3H_2O$ and ths in presence of free Hpic; (C) decomposition of $Pb(OAc)_2 \cdot 3H_2O$ and tu in presence of free H_2dipic. All scale bars = 1 μm.

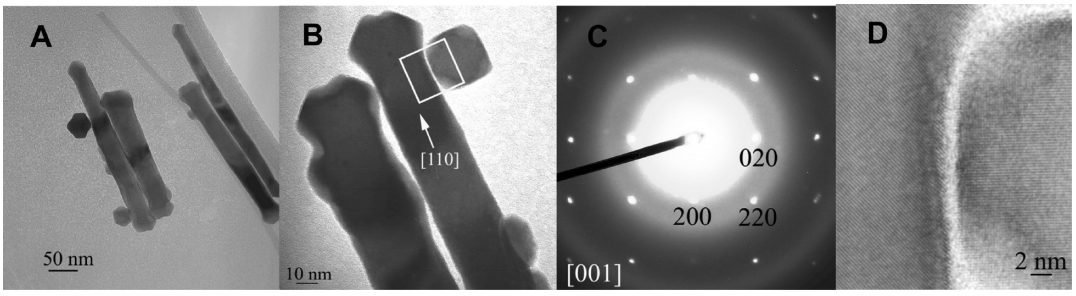

Figure 9. (A) BF TEM images of PbS nanoparticles synthesized from $Pb(OAc)_2$ and tu using OA as surfactant. (B) Enlarged view of the interfacial region between a rod and cubic nanocrystal, (C) SAED pattern from the nanorod showing the single crystal nature of the galena structure, (D) Expanded view of the interfacial region represented by the highlighted square.

Information). Reactions in presence of OA and a mixture of OA and TOA gave more interesting results. OA-assisted decompositions resulted in a mixture of cubes, truncated cubes and rods (Figure 9). The HR TEM images show that the nanoparticles are single crystals. Interestingly, in Figure 9D, one can see from the atomic planes that the nanorod and the nanocube have different orientations with the former having its long axis along [110] and the latter being directed along [100]. Increasing the amount of amine in the surfactant mixture resulted in a larger fraction of nanocubes. In a mixture of TOA and OA (5:1), nanocubes and rods with split ends were obtained (Figure 10). A detailed analysis of these rod-shaped nanoparticles indicates that the split starts from atomic distortions and dislocations (black arrows in the HR TEM image (Figure 10C)) that originated during nanocrystal growth. After ~8 nm of growth in the [110] direction, a twin boundary is formed. The single crystal rod continues to grow uniformly. After another ~30 nm growth, a split appears and a second nanorod forms (white arrows in HR TEM image (Figure 10D)). The SAED pattern recorded from this rod-shaped nanoparticle confirms such a split, showing a doubling of the diffraction spots along the axis of the splitting rod (Figure 10B). When the stress in the crystal structure created by the presence of linear and planar defects exceed some limit, the structure splits up.

Reactions with oleylamine produced nonuniform, micrometer-sized particles. Recent work by our group[3a,14c,26] and others[40] has shown the effect of air, oxygen, water vapor or acidity of reaction media in inducing crystal splitting and anisotropic growth of NPs. In particular, defect induced crystal splitting, which is often observed in systems where the growth rate is high, can also be promoted by the surfactant system and growth medium inhomogeneities.[39a]

dx.doi.org/10.1021/cm201064c |*Chem. Mater.* 2011, 23, 4158–4169

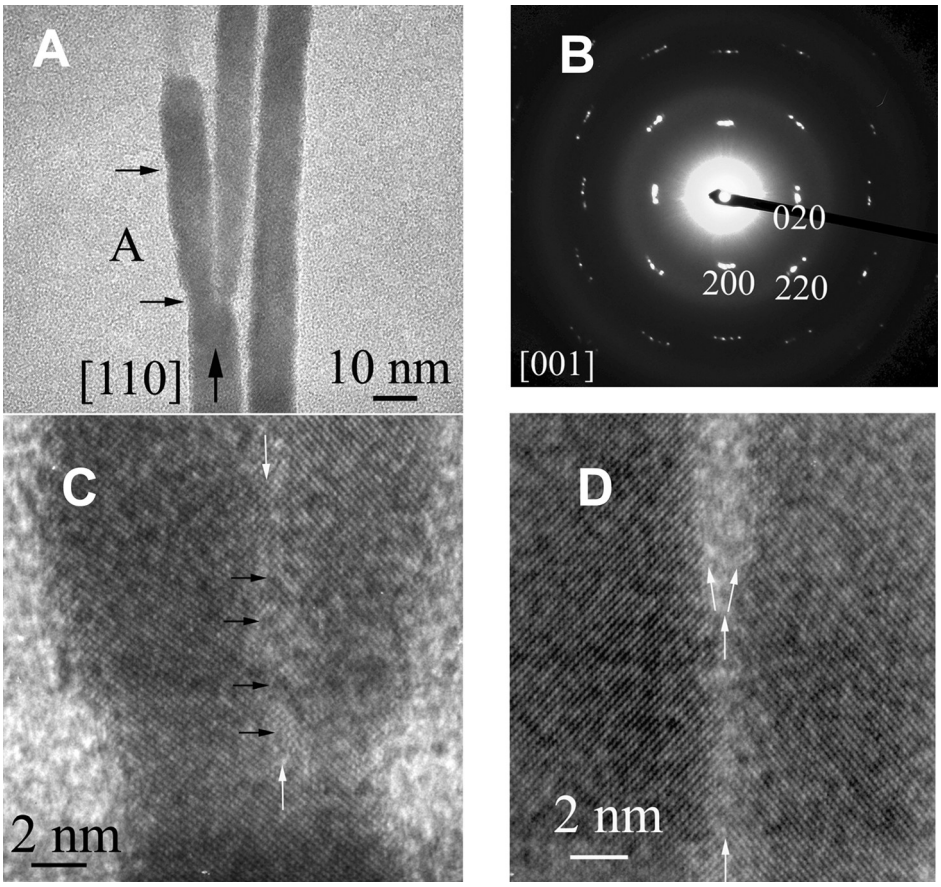

Figure 10. (A) Conventional BF TEM image of the nanorod split. (B) SAED pattern recorded from this rod-shaped nanoparticle confirm the direction of nanorod growth and the split. (C, D) HR TEM images of the area that is marked as A in the conventional TEM image A. Black arrows in C point to the dislocations. White arrows in D mark the area where the twin is formed and the splitting of the nanorod begins.

CONCLUSIONS

Aromatic carboxylate complexes of Pb(II) form stable adducts with thiourea or thiosemicarbazide. These compounds form readily because of the high affinity of Pb^{2+} ions for sulfur-based ligands and are stable under ambient conditions. They possess good solubility in common organic solvents and water. They can be used as molecular precursors for PbS semiconducting NPs in either aqueous or nonaqueous solvents. Although in all cases, pure PbS was obtained without additional S-based ligands, the addition of dodecanethiol to the surfactant system resulted in preferential and more uniform growth of cubic structures. The growth ratio between {100} and {111} faces of the nanocrystal can be altered by varying the polarity of the surfactant system and the addition of various stabilizers such as CTAB and SDS. In systems far from equilibrium high growth rates promote dendritic growth. Growth from multiple source precursors appeared to happen faster than that from single-source precursors, although similar shapes were obtained for both MSP and SSP systems. The dissolution growth in all cases is instigated at the atomic scale through linear and planar defects (dislocations and twins) leading to crystal splitting and regrowth, while faceted growth occurs often near equilibrium and the final faceting is dictated by the surfactant system that minimizes the Gibbs free energy of the growing surface.

ASSOCIATED CONTENT

Supporting Information. ^{13}C NMR data; thermogravimetric analyses of compounds **1a**, **1b**, **2a**, **2b**, **3a**, and **3b**; bond distances and angles for **2b**, **3a**, and **3b**; additional TEM and SEM images. This material is available free of charge via the Internet at http://pubs.acs.org.

AUTHOR INFORMATION

Corresponding Author

*E-mail: whitmir@rice.edu.

Present Addresses

‡Sandia National Laboratory, Livermore, California

⊥UCSB-MIT-Caltech Center For Collaborative Biotechnologies, Elings Hall, Santa Barbara, CA, 93106−5100

ACKNOWLEDGMENT

We gratefully acknowledge financial support from Welch Foundation (C-0976), the National Science Foundation (E-0411679), and the CRDF for a research grant (Award MTFP-1015). Also we would like to acknowledge Ron Benson from Rigaku Woodlands for his help with getting the single crystal data for compound **3a**.

REFERENCES

(1) (a) Darder, M.; Aranda, P.; Ruiz-Hitzky, E. *Adv. Mater.* **2007**, *19*, 1309. (b) Gao, H.; Ji, B.; Jager, I. L.; Arzt, E.; Fratzl, P. *Proc. Natl. Acad. Sci. U.S.A.* **2003**, *100*, 5597.(c) Mann, S. *Biomineralization:*

Principles and Concepts in Bioinorganic Materials Chemistry; Oxford University Press: Oxford, U.K., 2001; 240 pp; (d) Ould-Ely, T.; Luger, M.; Kaplan-Reinig, L.; Niesz, K.; Doherty, M.; Morse, D. E. *Nat. Protoc.* **2011**, *6*, 97.

(2) (a) Synder, R. C.; Studener, S.; Doherty, M. F. *AIChE J.* **2007**, *53*, 1510. (b) Synder, R. C.; Doherty, M. F. *AIChE J.* **2007**, *53*, 1337.

(3) (a) Ould-Ely, T.; Prieto-Centurion, D.; Kumar, A.; Guo, W.; Knowles, W. V.; Asokan, S. S.; Wong, M. S.; Rusakova, I.; Luttge, A.; Whitmire, K. H. *Chem. Mater.* **2006**, *18*, 1821. (b) Hou, Y.; Kondoh, H.; Ohta, T. *Cryst. Growth Des.* **2009**, *9*, 3119.

(4) Lovette, M. A.; Robben Browning, A.; Griffin, D. W.; Sizemore, J. P.; Snyder, R. C.; Doherty, M. F. *Ind. Eng. Chem. Res.* **2008**, *47*, 9812.

(5) Guenes, S.; Fritz, K. P.; Neugebauer, H.; Sariciftci, N. S.; Kumar, S.; Scholes, G. D. *Sol. Energy Mater. Sol. Cells* **2007**, *91*, 420.

(6) (a) Wang, S.; Yang, S. *Langmuir* **2000**, *16*, 389. (b) Yang, S.; Wang, S.; Fung, K. K. *Pure Appl. Chem.* **2000**, *72*, 119.

(7) Bierman, M. J.; Lau, Y. K. A.; Jin, S. *Nano Lett.* **2007**, *7*, 2907.

(8) Akhtar, J.; Malik, M. A.; O'Brien, P.; Helliwell, M. *J. Mater. Chem.* **2010**, *20*, 6116.

(9) (a) Jen-La Plante, I.; Zeid, T. W.; Yang, P.; Mokari, T. *J. Mater. Chem.* **2010**, *20*, 6612. (b) Sun, J.; Buhro, W. E. *Angew. Chem., Int. Ed.* **2008**, *47*, 3215.

(10) Luther, J. M.; Zheng, H.; Sadtler, B.; Alivisatos, A. P. *J. Am. Chem. Soc.* **2009**, *131*, 16851.

(11) Wang, S. F.; Feng, G.; Lue, M. K.; Zhou, G. J.; Zhang, A. Y. *J. Cryst. Growth* **2006**, *289*, 621.

(12) Wang, C.-W.; Liu, H.-G.; Bai, X.-T.; Xue, Q.; Chen, X.; Lee, Y.-I.; Hao, J.; Jiang, J. *Cryst. Growth Des.* **2008**, *8*, 2660.

(13) Biswas, K.; Rao, C. N. R. *Chem.—Eur. J.* **2007**, *13*, 6123.

(14) (a) Boudjouk, P.; Jarabek, B. R.; Simonson, D. L.; Seidler, D. J.; Grier, D. G.; McCarthy, G. J.; Keller, L. P. *Chem. Mater.* **1998**, *10*, 2358. (b) Duan, T.; Lou, W.; Wang, X.; Xue, Q. *Colloids Surf., A* **2007**, *310*, 86. (c) Mandal, T.; Stavila, V.; Rusakova, I.; Ghosh, S.; Whitmire, K. H. *Chem. Mater.* **2009**, *21*, 5617. (d) Kelly, A. T.; Rusakova, I.; Ould-Ely, T.; Hofmann, C.; Luettge, A.; Whitmire, K. H. *Nano Lett* **2007**, *7*, 2920. (e) Thurston, J. H.; Ely, T. O.; Trahan, D.; Whitmire, K. H. *Chem. Mater.* **2003**, *15*, 4407.

(15) Boulmaaz, S.; Papiernik, R.; Hubert-Pfalzgraf, L. G.; Septe, B.; Vaissermann, J. *J. Mater. Chem.* **1997**, *7*, 2053.

(16) Berhanu, D.; Govender, K.; Smyth-Boyle, D.; Archbold, M.; Halliday Douglas, P.; O'Brien, P. *Chem. Commun.* **2006**, 4709.

(17) Aslani, A.; Morsali, A.; Zeller, M. *Solid State Sci.* **2008**, *10*, 1591.

(18) (a) Salavati-Niasari, M.; Sobhani, A.; Davar, F. *J. Alloys Compd.* **2010**, *507*, 77. (b) Zhang, Z.; Lee, S. H.; Vittal, J. J.; Chin, W. S. *J. Phys. Chem. B* **2006**, *110*, 6649.

(19) Armarego, W. L. F.; Chai, C., *Purification of Laboratory Chemicals*, 5th ed.; Butterworth-Heinemann: New York, 2003.

(20) *Jade, XRD Pattern-Processing for the PC, 2.1*; MDI: Livermore, CA, 1994.

(21) *SMART, 5.04*; Bruker AXS Inc.: Madison, WI, 2002.

(22) Qian, D.-Q.; Shine, H. J.; Guzman-Jimenez, I. Y.; Thurston, J. H.; Whitmire, K. H. *J. Org. Chem.* **2002**, *67*, 4030.

(23) Sheldrick, G. *SADABS, 5.1*; University of Göttingen: Göttingen, Germany, 1997.

(24) Sheldrick, G. *SHELXTL*; University of Göttingen: Göttingen, Germany, 2001.

(25) (a) Harrowfield, J. M.; Lugan, N.; Marandi, F.; Shahverdizadeh, G. H.; Soudi, A. A. *Aust. J. Chem.* **2006**, *59*, 400. (b) Du, M.; Cai, H.; Zhao, X.-J. *Inorg. Chim. Acta* **2006**, *359*, 673.

(26) (a) Kelly, A. T.; Rusakova, I.; Ould-Ely, T.; Hofmann, C.; Luettge, A.; Whitmire, K. H. *Nano Lett.* **2007**, *7*, 2920. (b) Stavila, V.; Whitmire, K. H.; Rusakova, I. *Chem. Mater.* **2009**, *21*, 5456.

(27) Thurston, J. H.; Whitmire, K. H. *Abstracts of Papers, 225th ACS National Meeting*; New Orleans, LA, March 23−27, 2003; American Chemcial Society: Washington, D.C., 2003; INOR.

(28) (a) Sun, X. H.; Didychuk, C.; Sham, T. K.; Wong, N. B. *Nanotechnology* **2006**, *17*, 2925. (b) Wang, Y.; Meng, G.; Zhang, L.; Liang, C.; Zhang, J. *Chem. Mater.* **2002**, *14*, 1773.

(29) (a) Braun, P. V.; Osenar, P.; Tohver, V.; Kennedy, S. B.; Stupp, S. I. *J. Am. Chem. Soc.* **1999**, *121*, 7302. (b) Cho, K.-S.; Talapin, D. V.; Gaschler, W.; Murray, C. B. *J. Am. Chem. Soc.* **2005**, *127*, 7140. (c) Manna, L.; Milliron, D. J.; Meisel, A.; Scher, E. C.; Alivisatos, A. P. *Nat. Mater.* **2003**, *2*, 382. (d) Zhang, J.; Wang, Y.; Zheng, J.; Huang, F.; Chen, D.; Lan, Y.; Ren, G.; Lin, Z.; Wang, C. *J. Phys. Chem. B* **2007**, *111*, 1449.

(30) (a) Ghezelbash, A.; Korgel, B. A. *Langmuir* **2005**, *21*, 9451. (b) Manna, L.; Scher, E. C.; Alivisatos, A. P. *J. Am. Chem. Soc.* **2000**, *122*, 12700.

(31) Wang, Z. L. *J. Phys. Chem. B* **2000**, *104*, 1153.

(32) Zhang, C.; Kang, Z.; Shen, E.; Wang, E.; Gao, L.; Luo, F.; Tian, C.; Wang, C.; Lan, Y.; Li, J.; Cao, X. *J. Phys. Chem. B* **2006**, *110*, 184.

(33) Papatriantafyllopoulou, C.; Raptopoulou, C. P.; Terzis, A.; Janssens, J. F.; Manessi-Zoupa, E.; Perlepes, S. P.; Plakatouras, J. C. *Polyhedron* **2007**, *26*, 4053.

(34) Zhao, N.; Qi, L. *Adv. Mater.* **2006**, *18*, 359.

(35) Peng, Z.; Jiang, Y.; Song, Y.; Wang, C.; Zhang, H. *Chem. Mater.* **2008**, *20*, 3153.

(36) Jun, Y.-W.; Lee, J.-H.; Choi, J.-S.; Cheon, J. *J. Phys. Chem. B* **2005**, *109*, 14795.

(37) Marlow, F.; Muldarisnur; Sharifi, P.; Brinkmann, R.; Mendive, C. *Angew. Chem., Int. Ed.* **2009**, *48*, 6212.

(38) (a) Pacholski, C.; Kornowski, A.; Weller, H. *Angew. Chem., Int. Ed.* **2002**, *41*, 1188. (b) Tang, Z.; Kotov, N. A.; Giersig, M. *Science* **2002**, *297*, 237.

(39) (a) Sunagawa, I., *Crystals Growth, Morphology and Perfection*; Cambridge University Press: Cambridge, U.K., 2005. (b) Zhang, H.; Ha, D.-H.; Hovden, R.; Kourkoutis, L. F.; Robinson, R. D. *Nano Lett.* **2011**, *11*, 188. (c) Polshettiwar, V.; Baruwati, B.; Varma, R. S. *ACS Nano* **2009**, *3*, 728. (d) Wang, W.-S.; Zhen, L.; Xu, C.-Y.; Yang, L.; Shao, W.-Z. *Cryst. Growth Des.* **2008**, *8*, 1734.

(40) (a) Houtepen, A. J.; Koole, R.; Vanmaekelbergh, D.; Meeldijk, J.; Hickey, S. G. *J. Am. Chem. Soc.* **2006**, *128*, 6792. (b) Carbone, L.; Kudera, S.; Carlino, E.; Parak, W. J.; Giannini, C.; Cingolani, R.; Manna, L. *J. Am. Chem. Soc.* **2006**, *128*, 748.

(41) Afzaal, M.; Ellwood, K.; Pickett, N. L.; O'Brien, P.; Raftery, J.; Waters, J. *J. Mater. Chem.* **2004**, *14*, 1310.